# Using Electrochemical SERS to Measure the Redox Potential of Drug Molecules Bound to dsDNA – a Study of Mitoxantrone

*Marta Meneghello,[‡] Evanthia Papadopoulou,[†] Paolo Ugo,*[‡] and Philip N. Bartlett*[†]*

[†]*Chemistry, University of Southampton, Southampton, SO17 1BJ, UK*

[‡]*Department of Molecular Sciences and Nanosystems, University Ca'Foscari of Venice, via Torino 155, 30172 Venezia Mestre (Italy)*

KEYWORDS: Electrochemical SERS, Mitoxantrone, dsDNA, Redox reaction

**Abstract**

Interaction with DNA plays an important role in the biological activity of some anticancer drug molecules. In this paper we show that electrochemical surface enhanced Raman spectroscopy at sphere segment void gold electrodes can be used as a highly sensitive technique to measure the redox potential of the anticancer drug mitoxantrone bound to dsDNA. For this system we show that we can follow the redox reaction of the bound molecule and can extract the redox potential

for the molecule bound to dsDNA by deconvolution of the SER spectra recorded as a function of electrode potential. We find that mitoxantrone bound to dsDNA undergoes a 2 electron, 1 proton reduction and that the redox potential (-0.87 V *vs.* Ag/AgCl at pH 7.2) is shifted approximately 0.12 V cathodic of the corresponding value at a glassy carbon electrode. Our results also show that the reduced form of mitoxantrone remains bound to dsDNA and we are able to use the deconvoluted SER spectra of the reduced mitoxantrone as a function of electrode potential to follow the electrochemically driven melting of the dsDNA at more negative potentials.

## 1. Introduction

The biological and therapeutic activities of many compounds of pharmacological interest, including anticancer drugs [1] and antibiotics [2], correlate with their ability to bind to, or intercalate into, double stranded (ds) DNA. Consequently the interaction of drug molecules with dsDNA has been widely studied using a variety of techniques including circular dichroism, infra-red, Raman and UV-visible spectroscopies, NMR, SFM, mass spectrometry, and electrochemical techniques including potentiometry, cyclic voltammetry and differential pulse voltammetry, see Rauf *et al*. [3] and Sirajudin *et al.* [4] for recent reviews. These literature studies focus on the modes of binding of the drug molecule to the dsDNA, intercalation and/or minor and major groove binding and the binding constant for the drug molecule.

In addition, due to the ability of intercalators to selectively interact with dsDNA, they have been widely used as indicators for DNA hybridization utilizing fluorescence [5, 6], surface-enhanced Raman spectroscopy (SERS) [7] and electrochemical measurements [8-10]. An intercalator allows a “label free” DNA analysis because it selectively binds to the dsDNA,

removing the need to covalently attach the optical or electroactive indicator on the DNA sequence using complicated chemistry.

Many anticancer drugs are redox active and this redox activity is biologically important [1, 11]. For example anthracyclines are a class of anthraquinone derived drugs used in cancer therapy that can inhibit DNA and RNA synthesis after intercalation between the oligonucleotide bases [12, 13]. It has been reported that the one-electron reduction of quinone anticancer drugs is more damaging at a biological level because of the possibility of associated generation of reactive oxygen species [1]. In order to improve the understanding of the role of these interactions in the therapeutic action of these anti-cancer drugs, it is therefore important to be able to study how the properties of an electroactive intercalator change with its binding to DNA and/or as a consequence of changes in the redox state of the intercalator itself. Electrochemistry has been widely used both to study the redox reactions of anticancer drugs in solution and to study their interaction with DNA [2, 3, 14].

In this study we used the anticancer drug mitoxantrone (MTX) as a model compound to demonstrate the possibility of using electrochemical SERS as a very sensitive technique to study the redox behaviour of a drug molecule bound to dsDNA. MTX is an anthracycline analogue, Figure 1, and is one of the most promising anticancer drugs due the planar heterocyclic ring structure and side chains that allow interaction with dsDNA [15-17]. It has major clinical value in the treatment of certain types of cancer, such as lymphoma, acute leukaemia as well as ovarian and breast cancer [18-20]. MTX can be reduced enzymatically in living organism as well as *in vitro* at the electrode surface via one-electron or two-electron reduction processes [21]. The interactions of MTX with DNA and the electrochemistry of MTX have been extensively studied. For example the binding of MTX to dsDNA has been studied by UV-vis spectroscopy [15, 22-

25], FTIR [22], Raman [25, 26], circular dichroism [22, 23], fluorescence [23, 25], mass spectrometry [27], and calorimetry [28]. Electrochemical techniques have been used to study the redox reactions of MTX in solution, generally at carbon electrodes [29, 30], and to study the binding of MTX to dsDNA either in solution [25, 31, 32] or by using DNA modified electrodes [33, 34]. For example Oliveira Brett *et al*. [34] studied the electrochemistry of DNA modified glassy carbon electrodes with and without MTX present. The glassy carbon electrodes were modified by drying solutions of either single stranded or double stranded DNA on the surface. In the presence of MTX they found enhanced signals by differential pulse and square wave voltammetry for the oxidation of DNA bases, guanine and adenine, indicating DNA damage over several hours. Li *et al.* [25] studied the electrochemistry of MTX in solution with dsDNA using linear sweep voltammetry at glassy carbon. On addition of dsDNA they saw a significant decrease in the amplitude of the MTX reduction current and a small positive shift in the peak position. A similar effect is reported by Wang *et al*. [32] in their study using a waxed graphite working electrode. In both cases the shift is not quantified and is difficult to interpret as the voltammetry was irreversible.

**Figure 1 here**

Our approach builds on, and extends, earlier work using methylene blue as a binding agent to detect DNA hybridization and discrimination of mutations in the cystic fibrosis transmembrane conductance regulator (CFTR) gene utilizing an electrochemical melting procedure monitored by SERS [7]. In those studies, dsDNA was bound on a sphere segment void (SSV) surface and then exposed to a solution of methylene blue to bind to the double stranded DNA. SSV surfaces are thin, structured gold films with a regular array of spherical segment

cavities that provide tuneable and reproducible SERS enhancements and can also be used as electrodes [35, 36]. The binding of methylene blue to the double stranded DNA was monitored by recording the SERS signal of the intercalator bound to the DNA. Application of increasingly negative potential causes DNA denaturation, which is monitored by the changes in the intensity of methylene blue SERS spectra. As with many DNA binders, methylene blue is electrochemically active, therefore application of a negative potential causes its reduction to leucomethylene blue which has a different spectral signature compared to the oxidised form. For methylene blue the reduction occurs before the denaturation process, allowing the SERS intensity of the reduced form, leucomethylene blue, to be used to follow the electrochemically driven melting of the dsDNA.

In the present work we demonstrate the ability to use the electrochemical SERS to follow the redox reaction of the anticancer drug mitoxantrone when bound to dsDNA. This is a challenging goal since, in contrast with methylene blue, the MTX reduction process overlaps with the denaturation of the dsDNA. We show that we can still monitor the reduction process by monitoring the changes of the Raman spectra of the oxidised form of MTX. The results are correlated with the redox behaviour of mitoxantone measured by differential pulse voltammetry. Finally, we demonstrate that the MTX reduction and dsDNA melting can be well separated by operating at pH 5.

## 2. Experimental Section

All reagents used were of analytical grade and obtained from Sigma-Aldrich unless otherwise stated. Oligonucleotide synthesis was performed using standard methods by ATDBio Southampton, United Kingdom. The DNA probe (Table 1) had a three di-thiol linker at the 5’

end. This linker is chosen to ensure that the DNA probe remains attached to the electrode at high cathodic potentials.

**Table 1 here**

**2.1 Preparation of Sphere Segment Void (SSV) Substrates.** The fabrication and application of SSV substrates for SERS has been extensively described in the literature (see, for example, Abdelsalam *et al*. [35] and Cintra *et al*. [36]). In the present work an SSV surface fabricated using 600 nm sphere voids in a 480 nm thick film was selected as the plasmonics of this gold surface in aqueous solution are well suited to application with the 633 nm excitation used [37-39]. To prepare the SSV substrates a gold-chrome coated microscope slide was prepared by thermal vapour deposition of a 10 nm chromium adhesion layer followed by approximately 200 nm of gold onto a standard glass microscope slide. A monolayer template of 600 nm polystyrene spheres (Fisher Scientific as a 1% wt aqueous suspension) was formed at the surface using a convective assembly method. Gold was deposited through the template to a height of 480 nm at -0.72 V *vs*. SCE from a commercial gold plating solution (ECF 60, Metalor) containing 100 µL brightener (E3, Metalor) in 20 mL of plating solution. After deposition, the polystyrene spheres were removed by immersion in dimethylformamide (Rathburn, HPLC) for 30 min and the substrates were rinsed in deionised water before immediate use.

**2.2 DNA hybridization, binding with MTX and immobilisation on the SSV substrates.** A solution with both the DNA probe (5 µM) and target (10 µM) in 10 mM Tris buffer (pH 7.2), containing 0.3 M NaCl, was prepared and heated until 90 °C for 5 min; then 50 µM MTX was added. After slow cooling down to room temperature, the solution was diluted 1:5 with 10 mM

Tris/1 M NaCl buffer (pH 7.2) and SSV substrates were immersed in it for 24 h in order to allow the immobilization of the duplex DNA. Finally the substrates were passivated with 1 mM mercaptohexanol for 30 min, then washed with the buffer and kept in the Tris buffer until Raman spectra were recorded.

**2.3 Electrochemical SERS Measurements.** Electrochemical SERS experiments were carried out in a custom-built spectro-electrochemical Raman cell (Ventacon Ltd.) specifically designed for use with a Renishaw 2000 Raman microscope. It utilizes a horizontal geometry for viewing under the microscope, maintaining a thin 150 µL liquid film on the substrate. Electrochemical control is provided by a three-electrode arrangement inside the cell, where the SSV substrate is used as the working electrode, a platinum wire as the counter electrode and a silver/silver chloride pellet as the reference electrode ($E$(*vs*. SCE) = $E$(*vs*. Ag/AgCl) + 45 mV, value measured experimentally), Figure 2. In a typical electrochemical SERS experiment, the potential was swept at 1 mV/s from a starting potential of -0.3 to −1.3 V in 10 mM Tris buffer/0.1 M NaCl (pH 7.2). All electrochemical measurements were carried out using an EcoChemie AutolabIII potentiostat/galvanostat at room temperature.

**Figure 2 here**

**2.4 Raman instrumentation.** Raman spectra were acquired using a 50× objective on a Renishaw 2000 microscope instrument equipped with a 633 nm He-Ne laser and Prior XYZ stage controller. The laser power was 2.3 mW, spectra were recorded with an exposure time of 10-15 s and a spot size of 5 µm.

**2.5 Data analysis.** SERS spectra presented were baseline-corrected using a polynomial multipoint fitting function in Origin 9.1. The Raman intensities of the peaks are taken as height

above the baseline. A sigmoidal function was used to fit the melting profiles (Origin 9.1) and the first derivative of the fits was used to determine the melting points (inflection points of the melting curves). See below for details.

**2.6 UV-visible absorption spectra.** A solution with 50 µM MTX alone and one with 50 µM MTX and dsDNA (25 µM probe/50 µM target) were prepared in 10 mM Tris buffer (pH 7.2) containing 0.1 M NaCl. UV-visible absorption spectra were recorded using a spectrophotometer Varian (50 Probe). The baseline was subtracted using the Tris buffer as blank.

**2.7 Differential Pulse Voltammetry.** DPV experiments of MTX were performed at four different pH (5, 6.2, 7.2 and 9) using buffered solutions containing 10 mM acid/base and 0.1 M NaCl. Homemade glassy carbon electrodes (3 mm diameter, 0.071 $cm^2$ area) were polished by a standard procedure before each experiment: rubbed on metallographic abrasive paper (1200) and on polishing cloths (Bluehler) with alumina slurries (1.0 and 0.3 µM), followed by sonication in ethanol for 15 min. MTX was adsorbed on the surface of mirror like glassy carbon electrodes by dropping 4 µL aliquots of 1 mM MTX in ethanol on the electrode surface. The solvent was allowed to evaporate at room temperature for some minutes before the electrode was placed in the three-electrode cell with a homemade SCE as reference and a platinum mesh as counter electrode. The cell, connected to an Autolab PGSTAT30 potentiostat/galvanostat, was filled with 20 mL of the chosen buffer and deoxygenated by bubbling argon gas for 20 min. Three differential pulse voltammograms were acquired for each pH, using the Nova 1.6 software. The potential was scanned from -0.5 to -1 V using a modulation amplitude of 50 mV, a step potential of -5 mV and a step time of 0.5 s.

## 3. Results and Discussion

**3.1 Absorption spectra.** Figure 3 shows the visible absorption spectra of mitoxantrone in Tris buffer at pH 7.2: absorbance maxima of free MTX are located at 660 and 610 nm with a shoulder at 565 nm. It is well established that the absorption bands of the anthraquinone chromophore, usually in the visible region, are attributed to substitution of the anthraquinone ring by electron-donating substituents such as amino and hydroxyl groups [24]. In the MTX molecule, both hydroxyl and amino groups are present, and the absorbance bands can be attributed to the charge transition from the hydroxyl and amino substituents on the anthraquinone ring to the ring itself [22, 26]. When the MTX-DNA complex is formed, a bathochromic shift (red shift) of 20 nm is observed for both absorbance maxima, which move to 630 and 680 nm respectively (Figure 3, dotted line). The observed red shift agrees with previous literature reports [22, 25] and is consistent with reduced hydrogen bonding of the ring substituents upon binding to DNA; a similar bathochromic shift is observed for free MTX when using solvents with decreasing polarity [26].

Another phenomenon observable in Figure 3 is the change in intensity of the two main bands: upon binding to DNA, the band at 610 nm decreases, while the one at 660 nm increases. This effect has not been previously reported for MTX-DNA complexes, but Volanschi *et al.* reported that the shape of the MTX absorption spectrum is dependent on its concentration as a consequence of the formation of molecular aggregates in solution [40]; the band at 660 nm was assigned to the monomer and the band at 610 nm to the dimer of MTX. Such a role for the possible dimerization of MTX in concentrated solutions is confirmed by the evidence that at very low concentrations (up to 10 μM) the intensity of both absorption maxima is comparable (see also Fig. 4 in [25]), but with increasing concentration the band at 610 nm becomes more intense than the 660 nm band because of the formation of the dimer (this is the case in the free MTX

spectrum in Figure 3). Most probably, when MTX intercalates into dsDNA, the prevalent form is the monomer, so that the band at 660 nm (shifted to 680 nm by interaction with the dsDNA) strongly increases in intensity.

In the present context, it is worth noting that the absorbance maximum is always located between 600 and 700 nm and, consequently will be in resonance with the 633 nm laser used in our Raman experiments leading to a significant resonance contribution to the surface enhancement at the SSV substrates. Note that, at the same time, any fluorescence from the MTX will be heavily quenched due to the proximity of the molecule to the gold SSV surface.

**Figure 3 here**

**3.2 SERS Spectra.** SSV substrates with immobilised dsDNA and MTX as intercalator were prepared as described in the Experimental section. Note that in our experiments the dsDNA is held at the gold surface by six gold thiol bonds provided by the three dithiol groups joined to the DNA by a hexaethyleneglycol spacer (see Table 1). This ensures flexibility in the linkage of the dsDNA. The surface coverage is also low [41-43] (around 3 pmol $cm^{-2}$) to minimise interactions between adjacent dsDNA strands. Under these conditions we expect the interaction of the MTX with the dsDNA to be similar to that in free solution.

Figure 3 shows a typical SERS spectrum of MTX intercalated into dsDNA at an SSV substrate. Control experiments showed that, although MTX adsorbed on bare gold gave strong SER spectra, when the gold surface was coated in mercaptohexanol this was greatly suppressed (typically the spectra were around 40 times less intense at the mercaptohexanol coated surface). When SSV gold surfaces were modified with ssDNA and mercaptohexanol the MTX SER spectra were again either weak or not evident. In all cases MTX spectra for control electrodes

coated in mercaptohexanol, or ssDNA and mercaptohexanol, were >25 times less intense than those for the dsDNA modified electrodes discussed below indicating that for the dsDNA modified electrodes the spectra come from MTX associated with the dsDNA and not from MTX simply adsorbed at the electrode surface or associated with ssDNA. The spectra are in good agreement with published SER spectra for MTX at Ag colloids [44, 45]. The SERS signals for MTX are very intense, in particular the peak at 1300 $cm^{-1}$, which is used to monitor the changes in MTX Raman intensity in the experiments showed below. It is worth noting that the surface enhanced (resonant) Raman technique gives very high sensitivity - based on the laser spot size and the DNA surface coverage we estimate that the spectrum is acquired from around 20,000 dsDNA molecules. On the basis of previous studies [26, 44] the MTX bands were assigned as follows: 1300 $cm^{-1}$ ring stretch mode coupled with ν(C-O) mode of ring A; 1360 $cm^{-1}$ ν(C-O) motions coupling the vibration with the chelate system of the chromophore; 1445 and 1495 $cm^{-1}$ ν(C=C) motions; 1565 $cm^{-1}$ ring stretch vibration of the phenolic ring; 1642 $cm^{-1}$ ν(C=O) mode.

**Figure 4 here**

**Figure 5 here**

Figure 5 shows a typical set of SERS spectra of mitoxantrone collected in the course of an electrochemical SERS experiment scanning the potential between -0.6 and -1.2 V (*vs.* Ag/AgCl). In each experiment, the potential was ramped from a starting potential of -0.3 V to a final potential of -1.3 V (*vs.* Ag/AgCl), at a scan rate of 0.8 mV/s, and SER spectra were recorded every 25 mV. Upon application of the cathodic scan, the spectral intensity of MTX initially increases reaching the intensity maximum around -0.75 V and then decreases sharply. The initial increase in intensity is reversible and can be attributed to a change in the orientation

of the dye molecules with respect to the SSV surface, as a consequence of a potential-dependent change in the orientation of the DNA strands, as previously reported by Bartlett *et al.* [42]. On the other hand, the decrease in SERS signal at higher cathodic potentials (from around -0.8 V) is irreversible but does not arise from reductive desorption of the probe strands from the electrode surface (see below). Indeed, by using DNA probes designed with six thiols at the 5' end, reductive desorption does not become significant until the potential is taken more negative than -1.3 V *vs.* Ag/AgCl. This has been confirmed in earlier work showing that the target strands can be re-hybridised to the surface and SERS signal recovered [42].

If we look more closely at the spectra and compare those around -0.8 V with those at the more cathodic potentials (Figures 5 and 6), we can see that, in addition to the significant decrease in the intensity of the major band at 1300 $cm^{-1}$ together with a slight shift to lower wavenumber, there are significant changes in the relative intensities of the other bands. The band at 1642 $cm^{-1}$, attributed to the C=O stretching mode, disappears after -0.9 V: this would be consistent with reduction of the quinone groups of the anthraquinone ring at negative potential (see Scheme 1). Moreover, as shown in Figure 6, when the applied potential is around -0.9 V, a new band at 1340 $cm^{-1}$ appears and, sweeping the potential toward more negative values, it becomes more intense compared with the main band at 1300 $cm^{-1}$. The band at 1340 $cm^{-1}$ can be assigned to the aromatic ring stretching of the anthracene structure, since the reduction of MTX leads to gain of aromaticity between all the three rings. According to several authors, the main peak of anthracene is around 1400 $cm^{-1}$ [46-48], but it shifts to increasingly lower frequencies when the aromatic rings are substituted with more electron-donor groups, as in the case of MTX. Therefore, we attribute these changes to the reduction of the intercalated MTX.

Unfortunately, there are no Raman or SERS spectra for the reduced form of MTX reported in the literature. However, the changes in the absorption spectra after chemical reduction of MTX, as reported by Enache *et al.* [31], indicate that we expect a reduced contribution from resonance in the SER enhancement upon reduction, consistent with our interpretation here. Indeed, by increasing the concentration of tetrabutylammonium hydroxide during the reduction, the absorbance maximum of MTX shifts toward higher wavelength, resulting in a considerable decrease of the absorbance at 633 nm [31].

**Figure 6 here**

The changes in intensity of the main MTX peak at 1300 $cm^{-1}$ can be plotted as a function of the applied potential (Figure 7) and fitted with the following sigmoidal function

$$I = I_{\max} + \frac{I_{min} - I_{\max}}{\left(1 + e^{\frac{E - E_m}{dE}}\right)} \quad (1)$$

where $I$ is the absolute spectral intensity of the band at 1300 $cm^{-1}$ at the applied potential $E$; $I_{min}$ and $I_{max}$ are the average intensity values at the plateaux for the sigmoidal curve; $E_m$ is the half wave potential when $I$ equals $(I_{max} - I_{min})/2$, and d$E$ is a constant that describes the sharpness of the curve (the gradient of the curve at $E_m$ is $(I_{max} - I_{min})/4dE$). The data from each experiment were normalised to their respective $I_{max}$ values before plotting the melting curves to allow direct comparison. Note that the half wave potential in Figure 7 is -875 mV *vs.* Ag/AgCl (average of three replicate measurements). This is more positive of the electrochemically driven melting potential measured for the same DNA sequence in previous work by our group (-990 mV *vs.* Ag/AgCl) using the target strand labelled with Texas Red, therefore we do not believe that the decrease in SERS intensity seen around -875 mV in the present experiments can be accounted

for by electrochemically driven melting of the dsDNA and loss of the intercalator from the electrode surface. We return to this point below. To support this interpretation, we investigated the pH dependence of the electrochemical SERS, since we know from the literature that the redox reaction for a quinone should be strongly pH-dependent [49], whereas the electrochemically driven melting of dsDNA is not [50].

**Figure 7 here**

**3.3 Effect of pH on MTX reduction.** It is well-known that in buffered aqueous media at acidic, neutral and alkaline pH, anthraquinones and other *para*-quinones undergo reversible two-electron, one proton or two proton reduction [51] in which the reduction potential changes with pH in a straightforward Nernstian manner [49]. For comparison, electrochemical SERS experiments with intercalated MTX were performed by using buffered solutions at pH 5 and 9, in addition to the typical pH used in DNA melting experiments, which is 7.2. The sigmoidal curves obtained at the three different pH are well separated from each other. In order to deconvolute the spectra at each pH and separate out effects of the redox reaction of the intercalated MTX from possible electrochemically driven melting of the dsDNA and loss of intercalated MTX or reduced MTX, the spectra acquired during the electrochemical SERS experiments ($\mathbf{x}_{\mathrm{mix}}$) were fitted with the following equation

$$\mathbf{x}_{\mathrm{mix}} = A\mathbf{x}_{\mathrm{ox}} + B\mathbf{x}_{\mathrm{red}} + \boldsymbol{\varepsilon} \qquad (2)$$

where $A$ and $B$ are constants at each pH and potential, the arrays $\mathbf{x}_{\mathrm{ox}}$ and $\mathbf{x}_{\mathrm{red}}$ (pairs of Raman shift and corresponding intensity data recorded at 1 $cm^{-1}$ intervals from 1200 to 1700 $cm^{-1}$) are the spectra of the oxidised and reduced forms of MTX, respectively, and $\boldsymbol{\varepsilon}$ are the residuals. For

the spectra for the oxidised form, $\mathbf{x}_{ox}$, at each pH the spectra at -0.675 V for pH 5, -0.75 V for pH 7 and -0.825 V for pH 9 were used. For the spectra for the reduced form, $\mathbf{x}_{red}$, at each pH the spectra at -0.975 V for pH 5, -1.05 V for pH 7, and -1.15 V for pH 9, in which the band at 1340 $cm^{-1}$ is clearly visible were used. Note that the parameters *A* and *B* were allowed to vary independently of each other.

The parameter *A*, which describes the proportion of oxidised MTX, can be plotted versus the applied potential to monitor the reduction process of MTX. Figure 8 shows the plots of parameter *A* at different pH: it shows the decrease in MTX oxidised form as the potential is swept negative. The three curves for the three different pH are well separated but have the same general shape and similar values for d*E* (22 mV). By fitting the data of each curve to equation (1) we obtain half wave potentials of -780, -870 and -950 mV (*vs.* Ag/AgCl) for pH 5, 7.2 and 9, respectively. These values should correspond to the pH dependent formal reduction potentials for the intercalated mitoxantrone and can be compared to those obtained by differential pulse voltammetry (see below).

**Figure 8 here**

In the same way, the reduction of MTX can be monitored by the increment of parameter *B* (increment of reduced form) in the same potential range in which the parameter *A* decreases.

**3.4 DPV measurements.** Preliminary cyclic voltammetric measurements with a glassy carbon disk electrode in 500 µM MTX in 10 mM Tris buffer, 1 M NaCl, pH 7.2 (results not shown), indicate that MTX undergoes a reversible (or slightly quasi-reversible) two-electron reduction process with $E_{1/2} = (E_{pc} + E_{pa})/2 =$ -0.770 V *vs.* SCE, $\Delta E_p = E_{pc} - E_{pa}$ equal to ≈35 mV at a scan rate of 0.1 V/s and 42 mV at 1.0 V/s, and with a reduction peak current which scales linearly

with the square root of the scan rate (from 0.1 to 1.0 V/s). On this basis, in order to study the dependence of the MTX reduction potential on pH, we performed a series of differential pulse voltammetric measurements. DPV signals were recorded at different pH for MTX deposited by drop casting on glassy carbon electrodes (solubility in water is 89 mg/mL), Figure 9. The reduction peak potential shifts cathodic with increasing pH by approximately 30 mV/pH unit and at pH 7.2 the peak potential is -0.790 V *vs.* SCE, corresponding to a formal potential for the adsorbed MTX of -0.760 V *vs.* SCE taking account of the DPV pulse amplitude (using $E_p = E°' - \Delta E_p/2$, where $\Delta E_p$ is the pulse amplitude, 0.05 V). This value is in good agreement with the formal potential of the MTX evaluated above by cyclic voltammetry from the mid-peak potential.

**Figure 9 here**

These results indicate that, in the pH range investigated here, the reduction of MTX follows a two-electron, one-proton mechanism, Figure 10.

**Figure 10 here**

Figure 11 shows a comparison of the formal potentials for the intercalated MTX derived from the analysis of the electrochemical SERS data and for the MTX adsorbed on glassy carbon obtained from the DPV experiments as a function of solution pH. Both sets of data show essentially the same shift with pH, around 30 mV per pH unit, consistent with a $2e^-/1H^+$ redox reaction. There is an approximately constant offset between the two with the formal potentials obtained from the electrochemical SERS experiments for the intercalated DNA shifted by 110 to 120 mV to more negative potentials. It is not surprising that the values are different given the different environments of the MTX in the two cases. The cathodic shift indicates that

intercalation in dsDNA stabilises the oxidised form, relative to the reduced form, more than adsorption on the GC surface. The stabilisation effect of MTX on the double stranded DNA is discussed below.

**Figure 11 here**

The results presented so far show that we can obtain the redox potential for MTX bound to dsDNA by deconvolution of the SER spectra for the oxidised and reduced forms of MTX as a function of potential. The results also demonstrate that the reduced form of MTX remains bound to the dsDNA at the surface since we see SERS for this species at the more negative potential.

**3.5 *E*-melting.** At more negative potentials the SERS signal for MTX around 1300 $cm^{-1}$ falls to zero (see for example Figure 7 at potentials beyond -1.05 V *vs.* Ag/AgCl). This corresponds to the electrochemically driven melting (*E*-melting) of the dsDNA and subsequent loss of the intercalated reduced MTX from the SSV surface. We can follow this process using the results for the parameter *B* from our deconvolution of the spectra using equation (2) since this corresponds to the contribution from the reduced MTX. Figure 12 shows a plot of *B* as a function of the applied potential for the three different pH. It is pleasing that three sets of data are essential identical, as expected if the *E*-melting of the dsDNA is pH-independent.

The solid curves were obtained by fitting the B values to equation (1) and give a melting potential, $E_m$, of around -1.12 V *vs.* Ag/AgCl. The *E*-melting potential measured in other work of our group for this same DNA sequence labelled with Texas Red was -0.99 V *vs.* Ag/AgCl. The cathodic shift in melting potential of 120 mV seen with MTX is consistent with the generally observed stabilisation of dsDNA by interaction with intercalating agents [52]. Indeed, thermal melting studies showed that the melting temperature increases when intercalators were inserted

into the DNA duplex, and that this increase is even sharper when two or more molecules are bound to the same oligonucleotide because of a cooperative stabilization [53, 54].

**Figure 12 here**

## 4. Conclusions.

Our results show that electrochemical SERS at sphere segment void electrodes is a highly sensitive technique to probe the interaction of drug molecules, such as mitoxantrone, with double stranded DNA. We have shown that we can follow the redox reaction of the bound molecule using spectra acquired from around 20,000 dsDNA molecules, and that we can extract the redox potential for molecule in the bound state by deconvolution of the spectra.

For mitoxantrone we find that the redox potential for the molecule bound to dsDNA is -0.87 V *vs.* Ag/AgCl at 7.2. This is around 0.12 V cathodic of the corresponding value for the molecule adsorbed on glassy carbon. In addition, we find that the redox potential is pH dependent, shifting by approximately 30 mV per pH unit as expected for a 2 electron, 1 proton reaction.

Our results also show that the reduced form of mitoxantrone remains bound to the dsDNA. We are therefore able, using the deconvoluted spectra, to follow the electrochemically driven melting of the dsDNA at more negative potentials. We find that binding of the mitoxantrone stabilises the dsDNA. Comparison of our results at pH 5, 7.2 and 9 shows that this electrochemically driven melting is pH-independent over this range.

* Corresponding authors: Phone: 44-2380-592373 (PNB); 39-041-2348503 (PU). E-mail: p.n.bartlett@soton.ac.uk (PNB); ugo@unive.it (PU).

**Acknowledgement.** PNB gratefully acknowledges the receipt of a Wolfson Research Merit award. MM acknowledges the European program LLP Erasmus that permitted her to study at the University of Southampton during her Master degree.

## References

[1] P.L. Gutierrez, Front. Biosci., 5 (2000) D629-D638.
[2] J.W. Lown, Mol. Cell. Biochem., 55 (1983) 17-40.
[3] S. Rauf, J.J. Gooding, K. Akhtar, M.A. Ghauri, M. Rahman, M.A. Anwar, Khalid, J. Pharma. Biomed. Anal., 37 (2005) 205-217.
[4] M. Sirajuddin, S. Ali, A. Badshah, J. Photochem. Photobiol. B Biol., 124 (2013) 1-19.
[5] K.M. Ririe, R.P. Rasmussen, C.T. Wittwer, Anal. Biochem., 245 (1997) 154-160.
[6] T. Maruyama, T. Takata, H. Ichinose, N. Kamiya, H. Kuma, N. Hamasaki, H. Morita, M. Goto, Biotechnol. Prog., 21 (2005) 575-579.
[7] R.P. Johnson, J.A. Richardson, T. Brown, P.N. Bartlett, J. Am. Chem. Soc., 134 (2012) 14099-14107.
[8] E.L.S. Wong, J.J. Gooding, Aust. J. Chem., 58 (2005) 280-287.
[9] D. Ozkan, A. Erdem, P. Kara, K. Kerman, J.J. Gooding, P.N. Nielsen, M. Ozsoz, Electrochem. Commun., 4 (2002) 796-802.
[10] T. Endo, K. Kerman, N. Nagatani, Y. Takamura, E. Tamiya, Anal. Chem., 77 (2005) 6976-6984.
[11] D.J. Taatjes, G. Gaudiano, K. Katheryn Resing, T.H. Koch, J. Med. Chem., 40 (1997) 1276-1286.
[12] J.A. Plambeck, J.W. Lown, J. Electrochem. Soc., 131 (1984) 2556-2563.
[13] F. Traganos, D.P. Evenson, L. Staiano-Coico, Z. Darzynkiewicz, M.R. Melamed, Cancer Res., 40 (1980) 671-681.
[14] E. Palecek, M. Fojta, M. Tomschik, J. Wang, Biosens. Bioelectron., 13 (1998) 621-628.
[15] L.S. Rosenberg, M.J. Carvlin, T.R. Krugh, Biochemistry, 25 (1986) 1002-1008.
[16] K.J. Miller, D.D. Newlin, Biopolymers, 21 (1982) 633-652.
[17] K.C. Murdock, R.G. Child, P.F. Fabio, R.B. Angier, R.E. Wallace, F.E. Durr, R.V. Citarella, J. Med. Chem., 22 (1979) 1024-1030.
[18] R.K. Zee-Cheng, C.C. Cheng, J. Med. Chem., 21 (1978) 291-294.
[19] I.E. Smith, R. Stuartharris, N. Pavlidis, T. Bozek, Cancer Treat. Rev., 10 (1983) 37-40.
[20] T.D. Shenkenberg, D.D. Vonhoff, Ann. Intern. Med., 105 (1986) 67-81.
[21] Z. Fijalek, A. Snycerski, Acta Pol. Pharm., 51 (1994) 1-5.
[22] S. Agarwal, D.K. Jangir, R. Mehrotra, J. Photochem. Photobiol. B, 120 (2013) 177-182.
[23] S. Dogra, P. Awasthi, M. Nair, R. Barthwal, J. Photochem. Photobiol. B Biol., 123 (2013) 48-54.

[24] J. Kapuscinski, Z. Darzynkiewicz, Biochem. Pharmacol., 34 (1985) 4203-4213.
[25] N. Li, Y. Ma, C. Yang, L. Guo, X. Yang, Biophys. Chem., 116 (2005) 199-205.
[26] B.S. Lee, P.K. Dutta, J. Phys. Chem., 93 (1989) 5665-5672.
[27] B.S. Parker, T. Buley, B.J. Evison, S.M. Cutts, G.M. Neumann, M.N. Iskander, D.R. Phillips, J. Biol. Chem., 279 (2004) 18814-18823.
[28] J. Bhattacharyya, A. Basu, G.S. Kumar, J. Chem. Thermodynamics, 75 (2014) 45-51.
[29] Y. Mao, J. Hu, Q. Li, P. Xue, Analyst, 125 (2000) 2299-2302.
[30] A.M. Oliveira Brett, T.R.A. Macedo, D. Raimundo, M.H. Marques, S.H.P. Serrano, Anal. Chim. Acta, 385 (1999) 401-408.
[31] M. Enache, C. Bendic, E. Volanschi, Bioelectrochem., 72 (2008) 10-20.
[32] S. Wang, T. Peng, C.F. Yang, Biophys. Chem., 104 (2003) 239-248.
[33] A.N. Lad, Y.K. Agrawal, Instrument. Sci. Technol., 41 (2013) 325-334.
[34] A.M. Oliveira Brett, T.R.A. Macedo, D. Raimundo, M.H. Marques, S.H.P. Serrano, Biosens. Bioelectron., 13 (1998) 861-867.
[35] M.E. Abdelsalam, P.N. Bartlett, J.J. Baumberg, S. Cintra, T.A. Kelf, A.E. Russell, Electrochem. Commun., 7 (2005) 740-744.
[36] S. Cintra, M.E. Abdelsalam, P.N. Bartlett, J.J. Baumberg, T.A. Kelf, Y. Sugawara, A.E. Russell, Faraday Discuss., 132 (2006) 191.
[37] T.A. Kelf, Y. Sugawara, R.M. Cole, J.J. Baumberg, M.E. Abdelsalam, S. Cintra, S. Mahajan, A.E. Russell, P.N. Bartlett, Phys. Rev. B, 74 (2006) Art. No. 245415, 245411-245412.
[38] S. Mahajan, J.J. Baumberg, A.E. Russell, P.N. Bartlett, Phys. Chem. Chem. Phys, 9 (2007) 6016-6020.
[39] S. Mahajan, R.M. Cole, B.F. Soares, S.H. Pelfrey, A.E. Russell, J.J. Baumberg, P.N. Bartlett, J. Phys Chem., C, 113 (2009) 9284-9289.
[40] M. Enache, E. Volanski, Rev. Roum. Chim., 55 (2010) 255-262.
[41] R.P. Johnson, N. Gale, J.A. Richardson, T. Brown, P.N. Bartlett, Che. Sci., 4 (2013) 1625.
[42] S. Mahajan, J. Richardson, T. Brown, P.N. Bartlett, J. Am. Chem. Soc., 130 (2008) 15589-15601.
[43] S. Mahajan, J. Richardson, N.B. Gaied, Z. Zhao, T. Brown, P.N. Bartlett, Electroanalysis, 21 (2009) 2190-2197.
[44] I. Nabiev, G.D. Sockalingum, M. Manfait, A. Baranov, I. Chourpa, A. Beljebbar, J. Phys. Chem., 99 (1995) 1608-1613.
[45] D. Nieciecka, A. Krolikowska, P. Krysinski, Electrochimica Acta, 165 (2015) 430-442.
[46] G. Socrates, Infrared and Raman Characteristic Group Frequencies: Tables and Charts, 3rd ed., Wiley, Chichester, 2001.
[47] S.A. Asher, Anal. Chem., 56 (1984) 720-724.
[48] G.R. Loppnow, L. Shoute, K.J. Schmidt, A. Savage, R.H. Hall, J.T. Bulmer, Phil. Trans. R. Soc. Lond. A, 362 (2004) 2461–2476.
[49] P.S. Guin, S. Das, P.C. Mandal, Int. J. Electrochem., 2011 (2011) 1-22.
[50] R.P. Johnson, J.A. Richardson, T. Brown, P.N. Bartlett, Langmuir, 28 (2012) 5464-5470.
[51] J.Q. Chambers, Electrochemistry of quininones, in: S. Patai, Z. Rappoport (Eds.) The Chemistry of Quinoid Compounds", vol. 2, Wiley,, New York, USA, 1988, pp. 719-757.
[52] V.V. Filichev, E.B. Pedersen, DNA-conjugated organic chromophores in DNA stacking interactions, Wiley, Chichester, 2009.
[53] M.E. Ostergaard, M.C. Wamberg, E.B. Pedersen, Nucleos. Nucleot. Nucl., 30 (2011) 210-226.

[54] U.B. Christensen, E.B. Pedersen, Nucleic Acids Res., 30 (2002) 4918-4925.

**Table 1.** Oligonucleotide sequence used and the structures of the 3’ and 5’ anchors.

| | |
|---|---|
| Probe (5´-3´) | XXXH-GCAGCATCATTTGCTTTAGAGGC |
| Target (3´-5´) | CGTCGTAGTAAACGAAATCTCCG |

H = hexaethyleneglycol spacer; X = dithiol monomer

**a) Probe with 3' dithiol anchor**

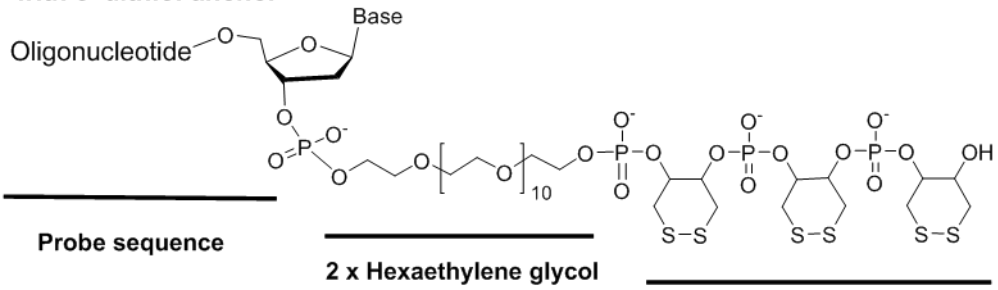


**b) Probe with 5' dithiol anchor**

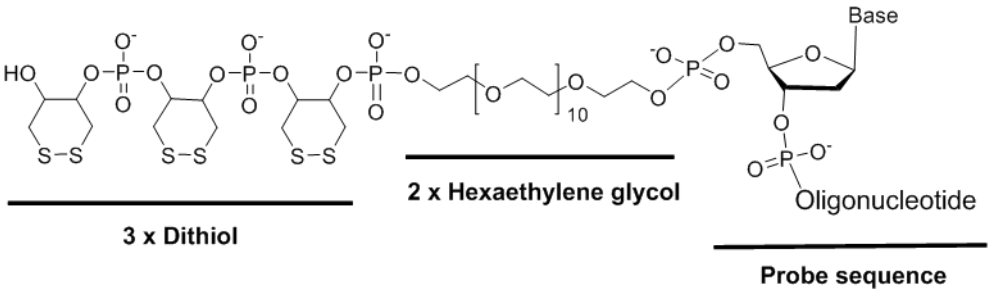

**Figure Legends**

**Figure 1.** Chemical structure of mitoxantrone (MTX). IUPAC name: 1,4-dihydroxy-5,8-bis[[2-[(2-hydroxyethyl)amino]ethyl]amino]-9,10-anthracenedione.

**Figure 2.** Schematic top view of the spectroelectrochemical cell used in this work. The cell is sealed by an optical window to give a 150 μl working volume and is ~2 cm in diameter.

**Figure 3.** The visible absorption spectra of 50 μM mitoxantrone in the absence (solid line) and presence of 25 μM dsDNA (dotted line). Both the spectra were recorded in 10 mM Tris/0.1 M NaCl buffer (pH 7.2).

**Figure 4.** SERS spectrum of mitoxantrone intercalated into dsDNA, acquired with 633 nm excitation laser. The spectrum was collected in 10 mM Tris/0.1 M NaCl buffer (pH 7.2) in static mode using one acquisition of 10 s, 5 μm spot size. The spectrum is normalised with collection time and laser power has been background subtracted for clarity.

**Figure 5.** SERS spectra of mitoxantrone bound to dsDNA at increasing negative potentials. The potential at the electrode surface was swept cathodic at a scan rate of 0.8 mV/s in a 10 mM Tris buffer (pH 7.2) containing 0.1 M NaCl. All potentials are measured against the Ag/AgCl reference electrode. The spectra have been background subtracted for clarity.

**Figure 6.** SERS spectra of mitoxantrone intercalated into dsDNA at different applied potentials (vs. Ag/AgCl), acquired with 633 nm laser. The potential at the electrode surface was swept cathodic at 0.8 mV/s in a 10 mM Tris buffer (pH 7.2) containing 0.1 M NaCl. Spectra have been

background subtracted and the intensity of each spectrum has been normalised to the intensity of the 1300 $cm^{-1}$ peak to make the comparison easier.

**Figure 7.** Three repeated experiments (shown by circles, triangles and squares) at pH 7.2 with mitoxantrone intercalated into dsDNA. The variation of the peak intensity close to 1300 $cm^{-1}$ is plotted as a function of applied potential. In each case the potential was swept cathodic at 0.8 mV/s in 10 mM Tris buffer (pH 7.2) containing 0.1 M NaCl. Spectra were acquired every 25 mV in static mode with a single 10 s acquisition, using a 633 nm laser.

**Figure 8.** Plot of the values of the A parameter obtained from the equation (2) as a function of applied potential for mitoxantrone intercalated into dsDNA at three different pH. In each case, the potential was swept cathodic at 0.8 mV/s in 10 mM buffer containing 0.1 M NaCl. SERS spectra were acquired every 25 mV in static mode with a single 10 s acquisition. In the graph, only the data used to construct the sigmoidal curves (see equation 1) are shown.

**Figure 9.** Differential pulse voltammograms of MTX adsorbed on glassy carbon at different pH. Potential was scanned between -0.5 and -1.0 V *vs.* SCE (modulation amplitude: 0.05 V, interval time 0.5 s).

**Figure 10.** Reduction scheme of mitoxantrone in aqueous media.

**Figure 11.** Reduction potential of mitoxantrone versus pH. The first set of data (●) was obtained through DPV experiments using MTX absorbed onto glassy carbon electrodes, while the second set (■) was obtained through SERS experiments using MTX intercalated into dsDNA (these data were converted in mV *vs.* SCE since the spectroelectrochemical cell has a Ag/AgCl electrode as

reference). For DPV the mean of three measurements is shown at each pH, errors were ± 2.5 mV; for SERS the values come from the fitting and the standard error on the fitted values was ± 5 mV or less. All the experiments were performed in buffer solutions containing 10 mM base/acid and 0.1 M NaCl.

**Figure 12.** Plot of the parameters *B* obtained with the equation (2) as a function of applied potential between -0.95 and -1.3 V for MTX intercalated into dsDNA at different pH. In each case, the potential was swept cathodic at 0.8 mV/s in 10 mM acid/base buffer containing 0.1 M NaCl. SERS spectra were acquired every 25 mV in static mode with a single 10 s acquisition. For each pH, parameters *B* were normalised to their respective maximum value to allow direct comparison.

Table of Contents Graphic